Model-Based Feedback Control of Autonomous Underwater Gliders

Naomi Ehrich Leonard and Joshua G. Graver

***Abstract*—We describe the development of feedback control for autonomous underwater gliders. Feedback is introduced to make the glider motion robust to disturbances and uncertainty. Our focus is on buoyancy-propelled, fixed-wing gliders with attitude controlled by means of active internal mass redistribution. We derive a nonlinear dynamic model of a nominal glider complete with hydrodynamic forces and coupling between the vehicle and the movable internal mass. We use this model to study stability and controllability of glide paths and to derive feedback control laws. For our analysis, we restrict to motion in the vertical plane and consider linear control laws. For illustration, we apply our methodology to a model of our own laboratory-scale underwater glider.**

***Index Terms*—Autonomous underwater vehicles, buoyancy control, glider control, glider dynamics, movable mass, underwater gliders.**

I. Introduction

In relation to existing methods of ocean sampling, autonomous underwater gliders offer a host of technical advantages: superior spatial and temporal measurement density, longer duration missions, and greater operational flexibility. These advantages are expected to be greatest when multiple gliders are operated cooperatively in a network [1]. The underwater glider concept, initially conceived by Henry Stommel [2], has motivated the development of several operational gliders, including the SLOCUM glider [3], the "Spray" glider [4] and the "Seaglider" [5]. These are all buoyancy-propelled, fixed-winged gliders which shift internal ballast to control attitude. Each has many useful features ranging from low operational and capital costs, and low noise and vibration to high reliability due to simplicity of design, minimal reliance on battery power, and low vulnerability of actuator mechanisms to the harsh effects of seawater.

In order for the advantages in ocean sampling using underwater gliders to be fully realized, an accurate and reliable glider control system should be developed. Most importantly, the use of feedback control provides a measure of robustness to uncertainty and disturbances. In this paper, we derive a nonlinear dynamic model and describe the first steps in development of model-based control for a class of underwater gliders, namely those with fixed external surfaces which can control buoyancy and center of gravity (CG). We emphasize an approach that is widely applicable rather than exclusively vehicle-specific; accordingly, this work complements the efforts on SLOCUM, Spray and Seaglider.

On SLOCUM, the ballast tanks are configured within the vehicle to provide the proper pitching moment during upwards and downwards glides [6], [3]. A sliding battery mass is used for fine adjustments in pitch and roll. Sensors measure depth, pitch, roll, and compass heading. Vehicle position at the surface is determined through GPS fix. The pitch angle, an assumed angle of attack, and a vertical speed computed from depth measurements are used to estimate the horizontal speed of the glider. The glider control system periodically checks the glider attitude and adjusts the position of the sliding battery mass. The timing of mass position adjustments can be changed depending on glider performance during the glide. Switching between downwards and upwards glides is performed open loop, i.e., the ballast is changed and the sliding mass is moved to a new position.

Sensing and control on other gliders is similar. For example, Spray performs active control of pitch and roll every 40 s using measured pitch and heading errors. In the case of pitch, a low-gain proportional control law is used, and in the case of heading, proportional plus integral control is used [4].

Our program initiated in this paper to develop a model-based, feedback control design methodology is intended to improve upon the currently implemented glider control strategies. A systematic design methodology that provides control in the full state-space is expected to make it possible to design glider controllers that require less experimentation and tuning and provide more robustness to fouling, payload changes and other uncertainties as compared to current techniques. Additionally, with a model-based approach, a dynamic observer can be designed to estimate states such as glider velocity. These estimated states could then be used to determine horizontal glider motion instead of the current methods which rely on assumptions of constant angle of attack. A model-based approach may also prove useful in determining optimal glider motions (see [7] for early work in this direction).

The dynamic glider model we derive here describes a glider with simple body and wing shape. Control is applied to two point masses inside the vehicle: the first point mass has variable mass but fixed position while the second point mass has fixed mass but variable position relative to the center of buoyancy. One control input changes the mass of the stationary point and another control input vector corresponds to the force applied to the movable mass. The model describes the nonlinear coupling between the vehicle and the shifting and changing mass. Analysis and control

Manuscript received October 3, 2000; revised June 8, 2001. This work was supported in part by the Office of Naval Research under Grant N00014-98-1-0649 and by the National Science Foundation under Grant BES-9502477.

The authors are with the Department of Mechanical and Aerospace Engineering, Princeton University, Princeton, NJ 08544 USA (e-mail: naomi@princeton.edu; jggraver@princeton.edu).

Publisher Item Identifier S 0364-9059(01)09800-4.

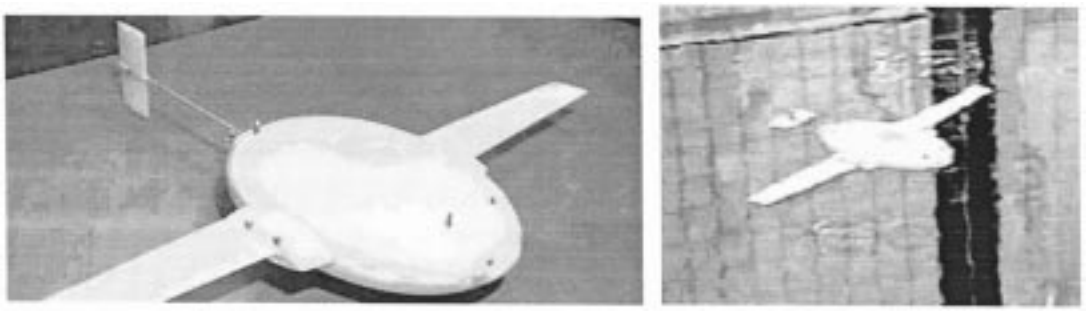

Fig. 1. Experimental, laboratory-scale underwater glider ROGUE.

law design is performed for the dynamics specialized to the vertical plane. Continuous feedback laws are developed. However, when energy is at a premium, we envision a scenario in which one might occasionally and temporarily turn off the active feedback control routine (including sensors), e.g., during periods of relative calm or when tight control is less critical.

The model we derive, although simplified, does capture the essential dynamic features of underwater gliding. The simplicity allows for development of general control design strategies. These strategies along with the insights gained from the development are expected to be relevant to the design of control laws for the more complex operational gliders. Feedback provides robustness to uncertainty, and this uncertainty may include unmodeled dynamics.

Specialization of the glider dynamics to the vertical plane constitutes a first step toward a systematic understanding and methodology for complete glider control design. In restricting to the vertical plane, we ignore, for example, challenges associated with currents traveling transverse to the motion of the vehicle. Analysis of tail volume requirements, heading corrections and the capabilities of shifting mass in this context will be next steps in developing methodology to meet these challenges. The successful SLOCUM glider experiments at LEO-15 during the summer of 2000 suggest promise for this program. In these experiments, SLOCUM performed excellent tracking in the presence of strong (transverse) currents [6].

Throughout the paper, we illustrate our results on a model of a small, laboratory-scale underwater glider called ROGUE (Remotely Operated Gliding Underwater Experiment) that we have built and that we operate in a freshwater tank and pool, see Fig. 1. In the first version of this glider, CG position is controlled by shifting a lead weight inside the vehicle [8]. In its most recent incarnation, ROGUE controls buoyancy and CG position by means of a distributed array of independently actuated ballast tanks (syringes).

In related and forthcoming work with colleagues, we address issues in optimal path planning for underwater gliders [7] and in coordinating control for multiple autonomous underwater vehicles [9], [10].

There is a great deal of literature on dynamics, stability, and control of airplanes, including [11], [12], [13]–[16], which is clearly of interest in the study of underwater gliders. We note, however, that added mass forces, variable buoyancy and controlled mass redistribution, which play a central role in our study of underwater gliders, are not typically relevant for airplanes and therefore not included in the airplane literature.

In Section II, we derive the equations of motion for a buoyancy-driven, fixed-wing underwater glider. Controllability and observability of steady glide paths in the vertical plane are studied in Section III. Linear control laws are developed in Section IV for stabilizing these glide paths in the presence of disturbances. A simulation of the controlled glider modeled to resemble ROGUE is also presented. We give final remarks in Section V.

II. Glider Dynamics

The variables used in this paper are defined in Table I.

A. Equations of Motion in 3-D

We model the underwater glider as a rigid body with fixed wings (and tail) immersed in a fluid with buoyancy control and controlled internal moving mass. We take the hull to be ellipsoidal with wings and tail attached so that the center of buoyancy (CB) is at the center of the ellipsoid. We assign a coordinate frame fixed on the vehicle body to have its origin at the CB and its axes aligned with the principle axes of the ellipsoid. Let body axis 1 lie along the long axis of the vehicle (positive in the direction of the nose of the glider), let body axis 2 lie in the plane of the wings and body axis 3 point in the direction orthogonal to the wings as shown in Fig. 2.

The total stationary mass, m_s, (also referred to as body mass) is the sum of three terms: m_h is a fixed mass that is uniformly distributed throughout the ellipsoid, m_w is a fixed point mass that may be offset from the CB, and m_b is the variable ballast point mass which is fixed in location at the CB. The vector from the CB to the point mass m_w is $\boldsymbol{r_w}$. The vector from the CB to the center of mass of the stationary mass $m_s = m_h + m_w + m_b$ is $\boldsymbol{r_s}$.

The moving internal point mass is $\overline{m}$. The vector $\boldsymbol{r_p}(t)$ describes the position of this mass with respect to the CB at time t. The total mass of the vehicle is then

$$m_v = m_h + m_w + m_b + \overline{m} = m_s + \overline{m}.$$

The mass of the displaced fluid is denoted m and we define $m_0 = m_v - m$ so that the vehicle is negatively (positively) buoyant if $-m_0$ is negative (positive). The different masses and position vectors are illustrated in Fig. 3.

TABLE I
DEFINITION OF VARIABLES

Name	Description
α	angle of attack, $\cos\alpha = v_1/\sqrt{v_1^2+v_3^2}$
$\boldsymbol{b}$	vehicle position vector from inertial frame
CB	center of buoyancy and origin of body frame
CG	center of gravity
D	drag force
$\boldsymbol{D_f}$	added mass cross term
$\boldsymbol{F_{ext}}$	external force on vehicle in body coordinates
$\boldsymbol{f_{ext}}$	external force on vehicle in inertial coordinates
$\boldsymbol{\mathcal{I}}$	identity matrix
$\boldsymbol{I}$	total mass/inertia matrix of vehicle/fluid system
$\boldsymbol{J_f}$	added inertia matrix
$\boldsymbol{J_h}$	inertia of hull (excludes inertia due to $\bar{m}$, m_w)
$\boldsymbol{J_s}$	inertia of stationary mass, $\boldsymbol{J_s} = \boldsymbol{J_h} - m_w\hat{\boldsymbol{r}}_{\boldsymbol{w}}\hat{\boldsymbol{r}}_{\boldsymbol{w}}$
$\boldsymbol{J}$	$\boldsymbol{J_s} + \boldsymbol{J_f}$
J_i	ith diagonal element of $\boldsymbol{J}$
L	lift force
$\boldsymbol{M}$	sum of body and added mass, $\boldsymbol{M} = m_s\boldsymbol{\mathcal{I}} + \boldsymbol{M_f}$
$\boldsymbol{M_f}$	added mass matrix
M_{DL}	viscous moment
m	mass of displaced fluid
$\bar{m}$	movable point mass
m_b	variable ballast mass located at CB
m_{fi}	ith diagonal element of $\boldsymbol{M_f}$
m_i	ith diagonal element of $\boldsymbol{M}$
m_h	uniformly distributed hull mass
m_s	stationary body mass, $m_s = m_h + m_w + m_b$
m_v	total vehicle mass, $m_v = m_s + \bar{m}$
m_w	point mass for nonuniform hull mass distribution
m_0	excess mass, $m_0 = m_v - m$
$\boldsymbol{\Omega}$	angular velocity in body coordinates
Ω_i	ith component of $\boldsymbol{\Omega}$
$\boldsymbol{P}$	total linear momentum in body coordinates
$\boldsymbol{P_p}$	linear momentum of $\bar{m}$ in body coordinates
$\boldsymbol{p}$	total linear momentum in inertial coordinates
$\boldsymbol{p_P}$	linear momentum of $\bar{m}$ in inertial coordinates
$\boldsymbol{\Pi}$	total angular momentum (body frame)
$\boldsymbol{\pi}$	total angular momentum (inertial frame)
$\boldsymbol{R}$	rotation matrix for vehicle orientation
$\boldsymbol{r_P}$	position of movable mass $\bar{m}$ in body coordinates
r_{Pi}	ith component of $\boldsymbol{r_P}$
$\boldsymbol{r_s}$	position vector from CB to center of mass m_s
$\boldsymbol{r_w}$	position vector from CB to m_w
θ	pitch angle
$\boldsymbol{T_{ext}}$	total external torque in body coordinates
$\boldsymbol{\tau_{ext}}$	pure external torque in inertial coordinates
T	total kinetic energy, $T = T_s + T_p + T_f$
T_f	kinetic energy of fluid
T_p	kinetic energy of movable point mass
T_s	kinetic energy of stationary body mass m_s
$\bar{\boldsymbol{u}}$	$(u_1\ u_2\ u_3)^T$, force on sliding point mass
$\boldsymbol{u}$	$(u_1\ u_2\ u_3\ u_4)^T$, vector of control inputs
u_4	controlled variable mass rate, $u_4 = \dot{m}_b$
V	speed in vertical plane, $V = \sqrt{(v_1^2+v_3^2)}$
V_d	desired speed in vertical plane
$\boldsymbol{v}$	velocity in body coordinates
v_i	ith component of $\boldsymbol{v}$
x, y, z	components of vehicle position vector $\boldsymbol{b}$
ξ	glide path angle, $\xi = \theta - \alpha$
ξ_d	desired glide path angle
z'	perpendicular distance to desired glide path

Let $\boldsymbol{J_h}$ denote the inertia matrix, with respect to the body frame, for the uniformly distributed mass m_h. Define the operator $\hat{}$ so that for a vector $\boldsymbol{x} = (x_1, x_2, x_3)^T$,

$$\hat{\boldsymbol{x}} = \begin{pmatrix} 0 & -x_3 & x_2 \\ x_3 & 0 & -x_1 \\ -x_2 & x_1 & 0 \end{pmatrix}.$$

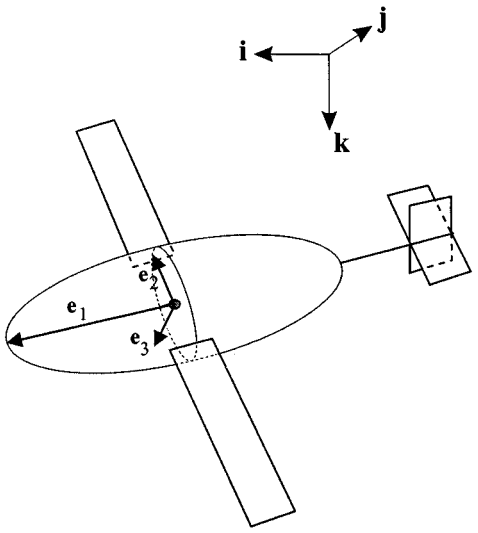

Fig. 2. Frame assignment on underwater glider.

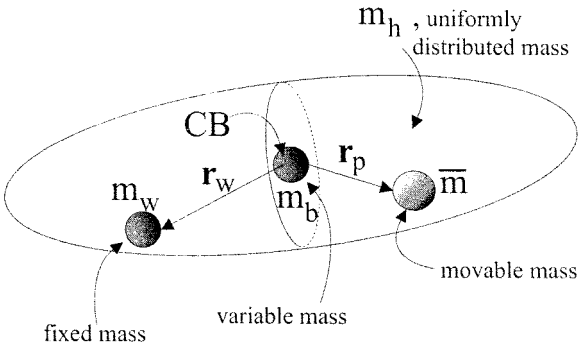

Fig. 3. Glider mass definitions.

Equivalently, for vector $\boldsymbol{y} = (y_1, y_2, y_3)^T$,

$$\hat{\boldsymbol{x}}\boldsymbol{y} = \begin{pmatrix} 0 & -x_3 & x_2 \\ x_3 & 0 & -x_1 \\ -x_2 & x_1 & 0 \end{pmatrix} \begin{pmatrix} y_1 \\ y_2 \\ y_3 \end{pmatrix} = \boldsymbol{x} \times \boldsymbol{y}$$

i.e., the operator $\hat{}$ maps a vector $\boldsymbol{x}$ to the (skew-symmetric) matrix representation of the vector cross product operator. The inertia matrix for the stationary (body) mass expressed with respect to body frame coordinates is

$$\boldsymbol{J_s} = \boldsymbol{J_h} - m_w\hat{\boldsymbol{r}}_{\boldsymbol{w}}\hat{\boldsymbol{r}}_{\boldsymbol{w}}.$$

Since the variable ballast mass m_b is a point mass located at the CB, it does not contribute to $\boldsymbol{J_s}$, and in particular $\boldsymbol{J_s}$ is a constant.

The orientation of the glider is given by the rotation matrix $\boldsymbol{R}$. $\boldsymbol{R}$ maps vectors expressed with respect to the body frame into inertial frame coordinates. The position of the glider $\boldsymbol{b} = (x, y, z)^T$ is the vector from the origin of the inertial frame to the origin of the body frame (vehicle CB) as shown in Fig. 4. The vehicle moves through the fluid with translational velocity $\boldsymbol{v} = (v_1, v_2, v_3)^T$ and angular velocity $\boldsymbol{\Omega} = (\Omega_1, \Omega_2, \Omega_3)^T$, expressed with respect to the body frame. [Note that we have diverged from the notation typical of the submarine literature where $\boldsymbol{v} = (u, v, w)^T$ and $\boldsymbol{\Omega} = (p, q, r)^T$. The notation that

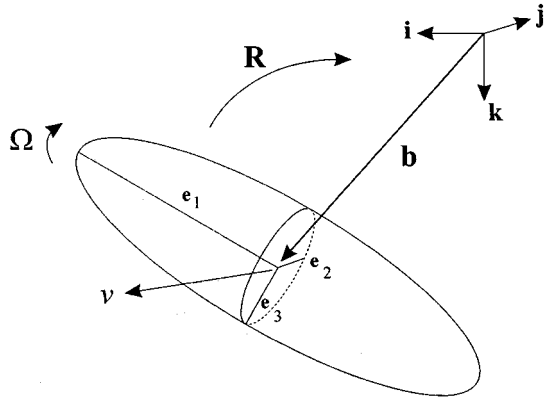

Fig. 4. Glider position and orientation variables.

we use here is taken from texts in classical mechanics such as [17] and is more convenient for the derivation and analysis.] In this notation, the kinematics of the glider are given by

$$\dot{R} = R\hat{\Omega} \tag{1}$$

$$\dot{b} = Rv. \tag{2}$$

Let $\boldsymbol{p}$ represent the total translational momentum of the vehicle-fluid system and $\boldsymbol{\pi}$ the total angular momentum of the system about the inertial coordinate origin, all expressed with respect to the inertial frame. Let $\boldsymbol{p_p}$ represent the total momentum of the movable point mass $\overline{m}$ with respect to the inertial frame. Then Newton's laws state that

$$\begin{aligned}\dot{\boldsymbol{p}} &= \sum_{i=1}^{I} \boldsymbol{f_{ext_i}} \\ \dot{\boldsymbol{\pi}} &= \sum_{i=1}^{I} \left(\boldsymbol{x_i} \times \boldsymbol{f_{ext_i}}\right) + \sum_{j=1}^{J} \boldsymbol{\tau_{ext_j}} \\ \dot{\boldsymbol{p}}_{\boldsymbol{p}} &= \overline{m}g\boldsymbol{k} + \sum_{k=1}^{K} \boldsymbol{f_{int_k}}\end{aligned} \tag{3}$$

where $\boldsymbol{k}$ is a unit vector pointing in the direction of gravity, $\boldsymbol{f_{ext_i}}$ is an external force applied to the system, and $\boldsymbol{\tau_{ext_j}}$ is a pure external torque. These external forces and torques include those due to gravity and buoyancy; however, gravity is included explicitly in the third set of equations as it is the only external force acting on the movable point mass. The force $\boldsymbol{f_{int_k}}$ is a force applied from the vehicle body onto the point mass (a control force). All vectors are expressed with respect to the inertial frame. The vector $\boldsymbol{x_i}$ locates the point of application of the force $\boldsymbol{f_{ext_i}}$ with respect to the inertial coordinate frame.

Let $\boldsymbol{P}$ be the momentum of the vehicle-fluid system expressed with respect to the body frame. Let $\boldsymbol{\Pi}$ be the total angular momentum about the origin of the body frame. Let $\boldsymbol{P_p}$ represent the point mass momentum with respect to the body frame. Then

$$\boldsymbol{p} = \boldsymbol{RP} \tag{4}$$

$$\boldsymbol{\pi} = \boldsymbol{R\Pi} + \boldsymbol{b} \times \boldsymbol{p} \tag{5}$$

$$\boldsymbol{p_p} = \boldsymbol{RP_p}. \tag{6}$$

Differentiating (4)–(6) and using the kinematic expressions (2) and (1) gives

$$\begin{aligned}\dot{\boldsymbol{p}} &= \boldsymbol{R}\left(\dot{\boldsymbol{P}} + \hat{\Omega}\boldsymbol{P}\right) \\ \dot{\boldsymbol{\pi}} &= \boldsymbol{R}\left(\dot{\boldsymbol{\Pi}} + \hat{\Omega}\boldsymbol{\Pi}\right) + \boldsymbol{Rv} \times \boldsymbol{p} + \boldsymbol{b} \times \dot{\boldsymbol{p}} \\ \dot{\boldsymbol{p}}_{\boldsymbol{p}} &= \boldsymbol{R}\left(\dot{\boldsymbol{P}}_{\boldsymbol{p}} + \hat{\Omega}\boldsymbol{P}_{\boldsymbol{p}}\right).\end{aligned} \tag{7}$$

Substituting (3) into (7) for the rate of change of inertial momenta gives the following dynamic equations in body coordinates:

$$\dot{\boldsymbol{P}} = \boldsymbol{P} \times \boldsymbol{\Omega} + \boldsymbol{R}^T \sum_{i=1}^{I} \boldsymbol{f_{ext_i}} \tag{8}$$

$$\begin{aligned}\dot{\boldsymbol{\Pi}} = \boldsymbol{\Pi} \times \boldsymbol{\Omega} + \boldsymbol{P} \times \boldsymbol{v} + \boldsymbol{R}^T \left(\sum_{i=1}^{I} (\boldsymbol{x_i} - \boldsymbol{b}) \times \boldsymbol{f_{ext_i}}\right) \\ + \boldsymbol{R}^T \sum_{j=1}^{J} \boldsymbol{\tau_{ext_j}}\end{aligned} \tag{9}$$

$$\dot{\boldsymbol{P}}_{\boldsymbol{p}} = \boldsymbol{P}_{\boldsymbol{p}} \times \boldsymbol{\Omega} + \overline{m}g(\boldsymbol{R}^T\boldsymbol{k}) + \tilde{\boldsymbol{u}} \tag{10}$$

where $\tilde{\boldsymbol{u}} = \boldsymbol{R}^T \sum_{k=1}^{K} \boldsymbol{f_{int_k}}$ is the internal force acting on the point mass in body coordinates. Let

$$\overline{\boldsymbol{u}} = \begin{pmatrix} u_1 \\ u_2 \\ u_3 \end{pmatrix} = \boldsymbol{P}_{\boldsymbol{p}} \times \boldsymbol{\Omega} + \overline{m}g(\boldsymbol{R}^T\boldsymbol{k}) + \tilde{\boldsymbol{u}} \tag{11}$$

so that

$$\dot{\boldsymbol{P}}_{\boldsymbol{p}} = \overline{\boldsymbol{u}}.$$

To derive expressions for $\boldsymbol{P}$, $\boldsymbol{\Pi}$, and $\boldsymbol{P_p}$, we determine the total kinetic energy of the glider-fluid system. The kinetic energy T_s of the rigid body with mass m_s and inertia matrix $\boldsymbol{J_s}$ is

$$T_s = \tfrac{1}{2}\begin{pmatrix} \boldsymbol{v} \\ \boldsymbol{\Omega} \end{pmatrix} \cdot \begin{pmatrix} m_s\mathcal{I} & -m_s\hat{\boldsymbol{r}}_{\boldsymbol{s}} \\ m_s\hat{\boldsymbol{r}}_{\boldsymbol{s}} & \boldsymbol{J_s} \end{pmatrix} \begin{pmatrix} \boldsymbol{v} \\ \boldsymbol{\Omega} \end{pmatrix}.$$

Let $\boldsymbol{v_p}$ be the absolute velocity of the movable point mass $\overline{m}$ expressed in body coordinates. Given that the velocity of $\overline{m}$ relative to the body frame is $\dot{\boldsymbol{r}}_{\boldsymbol{p}}$, we compute

$$\boldsymbol{v_p} = \boldsymbol{v} + \dot{\boldsymbol{r}}_{\boldsymbol{p}} + \boldsymbol{\Omega} \times \boldsymbol{r_p}. \tag{12}$$

The kinetic energy T_p of the movable point mass is then computed to be

$$\begin{aligned}T_p &= \frac{1}{2}\overline{m}\|\boldsymbol{v_p}\|^2 \\ &= \tfrac{1}{2}\begin{pmatrix} \boldsymbol{v} \\ \boldsymbol{\Omega} \\ \dot{\boldsymbol{r}}_{\boldsymbol{p}} \end{pmatrix} \cdot \begin{pmatrix} \overline{m}\mathcal{I} & -\overline{m}\hat{\boldsymbol{r}}_{\boldsymbol{p}} & \overline{m}\mathcal{I} \\ \overline{m}\hat{\boldsymbol{r}}_{\boldsymbol{p}} & -\overline{m}\hat{\boldsymbol{r}}_{\boldsymbol{p}}\hat{\boldsymbol{r}}_{\boldsymbol{p}} & \overline{m}\hat{\boldsymbol{r}}_{\boldsymbol{p}} \\ \overline{m}\mathcal{I} & -\overline{m}\hat{\boldsymbol{r}}_{\boldsymbol{p}} & \overline{m}\mathcal{I} \end{pmatrix} \begin{pmatrix} \boldsymbol{v} \\ \boldsymbol{\Omega} \\ \dot{\boldsymbol{r}}_{\boldsymbol{p}} \end{pmatrix}.\end{aligned}$$

Kirchhoff [18] showed that the kinetic energy of an unbounded volume of ideal fluid due to the motion of an immersed rigid body takes the form

$$T_f = \frac{1}{2}\begin{pmatrix} \boldsymbol{v} \\ \boldsymbol{\Omega} \end{pmatrix} \cdot \begin{pmatrix} \boldsymbol{M_f} & \boldsymbol{D_f^T} \\ \boldsymbol{D_f} & \boldsymbol{J_f} \end{pmatrix} \begin{pmatrix} \boldsymbol{v} \\ \boldsymbol{\Omega} \end{pmatrix}$$

where $\boldsymbol{M_f}$ is the added mass matrix, $\boldsymbol{J_f}$ is the added inertia matrix, and $\boldsymbol{D_f}$ is the added cross term. These matrices depend upon the external shape of the body and the density of the fluid. This form of kinetic energy comes from a potential flow solution in which the fluid is assumed to be inviscid, incompressible, irrotational and motionless at infinity. We incorporate viscous effects into the model as external forces and torques (lift and drag) below.

We assume that at low angle of attack, the contribution of the wings is dominated by lift and drag forces. Thus, we make the simplifying assumption that the added mass and inertia terms can be computed solely from the vehicle hull. These assumptions are not so critical for the analysis in this paper, especially since it is expected that feedback control will provide robustness to unmodeled dynamics. Nonetheless, it may be of interest in future work to consider more detailed modeling of added mass associated with the hull plus wings using methods such as from computational fluid dynamics.

The total vehicle fluid kinetic energy $T = T_s + T_p + T_f$ is computed to be

$$T = \frac{1}{2}\begin{pmatrix}\boldsymbol{v}\\ \boldsymbol{\Omega}\\ \dot{\boldsymbol{r}}_{\boldsymbol{p}}\end{pmatrix}\cdot \boldsymbol{I}\begin{pmatrix}\boldsymbol{v}\\ \boldsymbol{\Omega}\\ \dot{\boldsymbol{r}}_{\boldsymbol{p}}\end{pmatrix}$$

$$\boldsymbol{I} = \begin{pmatrix}(m_s+\overline{m})\mathcal{I}+\boldsymbol{M_f} & -\overline{m}\hat{\boldsymbol{r}}_{\boldsymbol{p}} - m_s\hat{\boldsymbol{r}}_{\boldsymbol{s}} + \boldsymbol{D_f^T} & \overline{m}\mathcal{I}\\ \overline{m}\hat{\boldsymbol{r}}_{\boldsymbol{p}} + m_s\hat{\boldsymbol{r}}_{\boldsymbol{s}} + \boldsymbol{D_f} & \boldsymbol{J_s} - \overline{m}\hat{\boldsymbol{r}}_{\boldsymbol{p}}\hat{\boldsymbol{r}}_{\boldsymbol{p}} + \boldsymbol{J_f} & \overline{m}\hat{\boldsymbol{r}}_{\boldsymbol{p}}\\ \overline{m}\mathcal{I} & -\overline{m}\hat{\boldsymbol{r}}_{\boldsymbol{p}} & \overline{m}\mathcal{I}\end{pmatrix}.$$

We can then compute momenta as

$$\begin{aligned}\boldsymbol{P} &= \frac{\partial T}{\partial \boldsymbol{v}} = (m_s\mathcal{I}+\boldsymbol{M_f})\boldsymbol{v} + \boldsymbol{D_f^T}\boldsymbol{\Omega} + m_s\boldsymbol{\Omega}\times\boldsymbol{r_s}\\ &\quad + \overline{m}(\boldsymbol{v}+\boldsymbol{\Omega}\times\boldsymbol{r_p}+\dot{\boldsymbol{r}}_{\boldsymbol{p}}),\\ \boldsymbol{\Pi} &= \frac{\partial T}{\partial \boldsymbol{\Omega}} = \boldsymbol{D_f}\boldsymbol{v} + (\boldsymbol{J_s}+\boldsymbol{J_f})\boldsymbol{\Omega} + m_s\boldsymbol{r_s}\times\boldsymbol{v}\\ &\quad + \overline{m}\hat{\boldsymbol{r}}_{\boldsymbol{p}}(\boldsymbol{v}+\boldsymbol{\Omega}\times\boldsymbol{r_p}+\dot{\boldsymbol{r}}_{\boldsymbol{p}}),\\ \boldsymbol{P_p} &= \frac{\partial T}{\partial \dot{\boldsymbol{r}}_{\boldsymbol{p}}} = \overline{m}(\boldsymbol{v}+\boldsymbol{\Omega}\times\boldsymbol{r_p}+\dot{\boldsymbol{r}}_{\boldsymbol{p}}).\end{aligned}$$

Since the vehicle hull is ellipsoidal (we neglect the wings in this instance), $\boldsymbol{M_f}$ and $\boldsymbol{J_f}$ are diagonal and $\boldsymbol{D_f} = \boldsymbol{0}$. Let $\boldsymbol{M_f} = \mathrm{diag}(m_{f1}, m_{f2}, m_{f3})$ and $\boldsymbol{J_f} = \mathrm{diag}(J_{f1}, J_{f2}, J_{f3})$. Define

$$\boldsymbol{M} = m_s\mathcal{I} + \boldsymbol{M_f}, \qquad \boldsymbol{J} = \boldsymbol{J_s} + \boldsymbol{J_f}$$

where $\mathcal{I}$ is the 3×3 identity matrix. Let $\boldsymbol{M} = \mathrm{diag}(m_1, m_2, m_3)$ and $\boldsymbol{J} = \mathrm{diag}(J_1, J_2, J_3)$. Furthermore, assume that $m_w = 0$ so that $\boldsymbol{r_s} = \boldsymbol{0}$. Then,

$$\begin{pmatrix}\boldsymbol{P}\\ \boldsymbol{\Pi}\\ \boldsymbol{P_p}\end{pmatrix} = \boldsymbol{I}\begin{pmatrix}\boldsymbol{v}\\ \boldsymbol{\Omega}\\ \dot{\boldsymbol{r}}_{\boldsymbol{p}}\end{pmatrix},$$

$$\boldsymbol{I} = \begin{pmatrix}\boldsymbol{M}+\overline{m}\mathcal{I} & -\overline{m}\hat{\boldsymbol{r}}_{\boldsymbol{p}} & \overline{m}\mathcal{I}\\ \overline{m}\hat{r}_{\boldsymbol{p}} & \boldsymbol{J} - \overline{m}\hat{\boldsymbol{r}}_{\boldsymbol{p}}\hat{\boldsymbol{r}}_{\boldsymbol{p}} & \overline{m}\hat{\boldsymbol{r}}_{\boldsymbol{p}}\\ \overline{m}\mathcal{I} & -\overline{m}\hat{\boldsymbol{r}}_{\boldsymbol{p}} & \overline{m}\mathcal{I}\end{pmatrix}. \quad (13)$$

Inverting the relationships (13) then gives the body velocities in terms of the body momenta:

$$\begin{pmatrix}\boldsymbol{v}\\ \boldsymbol{\Omega}\\ \dot{\boldsymbol{r}}_{\boldsymbol{p}}\end{pmatrix} = \boldsymbol{I}^{-1}\begin{pmatrix}\boldsymbol{P}\\ \boldsymbol{\Pi}\\ \boldsymbol{P_p}\end{pmatrix}, \quad (14)$$

$$\boldsymbol{I^{-1}} = \begin{pmatrix}\boldsymbol{M^{-1}} & \boldsymbol{0} & -\boldsymbol{M^{-1}}\\ \boldsymbol{0} & \boldsymbol{J^{-1}} & -\boldsymbol{J^{-1}}\hat{\boldsymbol{r}}_{\boldsymbol{p}}\\ -\boldsymbol{M^{-1}} & \hat{\boldsymbol{r}}_{\boldsymbol{p}}\boldsymbol{J^{-1}} & \boldsymbol{M^{-1}} - \hat{\boldsymbol{r}}_{\boldsymbol{p}}\boldsymbol{J^{-1}}\hat{\boldsymbol{r}}_{\boldsymbol{p}} + \frac{1}{\overline{m}}\mathcal{I}\end{pmatrix}.$$

To get the equations of motion in terms of body velocities, we differentiate (14) with respect to time. We assume that buoyancy is changed in a symmetric way (e.g., ballast is pumped on and off board in streams with the appropriate symmetry) so that there is negligible associated thrust or moment on the glider. Let the ballast control input u_4 be defined as

$$u_4 = \dot{m}_b. \quad (15)$$

Differentiating (14) then gives

$$\begin{pmatrix}\dot{\boldsymbol{v}}\\ \dot{\boldsymbol{\Omega}}\\ \ddot{\boldsymbol{r}}_{\boldsymbol{p}}\end{pmatrix} = \boldsymbol{I^{-1}}\begin{pmatrix}\dot{\boldsymbol{P}}\\ \dot{\boldsymbol{\Pi}}\\ \dot{\boldsymbol{P}}_{\boldsymbol{p}}\end{pmatrix} + \frac{d}{dt}(\boldsymbol{I^{-1}})\begin{pmatrix}\boldsymbol{P}\\ \boldsymbol{\Pi}\\ \boldsymbol{P_p}\end{pmatrix} \quad (16)$$

where

$$\frac{d}{dt}(\boldsymbol{I^{-1}}) = \begin{pmatrix}\boldsymbol{0} & \boldsymbol{0} & \boldsymbol{0}\\ \boldsymbol{0} & \boldsymbol{0} & -\boldsymbol{J^{-1}}\dot{\hat{\boldsymbol{r}}}_{\boldsymbol{p}}\\ \boldsymbol{0} & \dot{\hat{\boldsymbol{r}}}_{\boldsymbol{p}}\boldsymbol{J^{-1}} & -\dot{\hat{\boldsymbol{r}}}_{\boldsymbol{p}}\boldsymbol{J^{-1}}\hat{\boldsymbol{r}}_{\boldsymbol{p}} - \hat{\boldsymbol{r}}_{\boldsymbol{p}}\boldsymbol{J^{-1}}\dot{\hat{\boldsymbol{r}}}_{\boldsymbol{p}}\end{pmatrix}. \quad (17)$$

With the substitution into (16) of (8)–(11) for the derivatives $\dot{\boldsymbol{P}}$, $\dot{\boldsymbol{\Pi}}$ and $\dot{\boldsymbol{P}}_{\boldsymbol{p}}$, (17) for $d/dt(\boldsymbol{I^{-1}})$ and (13) for the relationship between momenta and velocity, the complete equations of motion for the underwater glider moving in three-dimensional space are

$$\begin{pmatrix}\dot{\boldsymbol{R}}\\ \dot{\boldsymbol{b}}\\ \dot{\boldsymbol{\Omega}}\\ \dot{\boldsymbol{v}}\\ \dot{\boldsymbol{r}}_{\boldsymbol{p}}\\ \dot{\boldsymbol{P}}_{\boldsymbol{p}}\\ \dot{m}_b\end{pmatrix} = \begin{pmatrix}\boldsymbol{R}\hat{\boldsymbol{\Omega}}\\ \boldsymbol{R}\boldsymbol{v}\\ \boldsymbol{J^{-1}}\overline{\boldsymbol{T}}\\ \boldsymbol{M^{-1}}\overline{\boldsymbol{F}}\\ \frac{1}{\overline{m}}\boldsymbol{P_p} - \boldsymbol{v} - \boldsymbol{\Omega}\times\boldsymbol{r_p}\\ \overline{\boldsymbol{u}}\\ u_4\end{pmatrix}, \quad (18)$$

$$\begin{aligned}\overline{\boldsymbol{T}} &= (\boldsymbol{J\Omega} + \hat{\boldsymbol{r}}_{\boldsymbol{p}}\boldsymbol{P_p})\times\boldsymbol{\Omega} + \boldsymbol{M}\boldsymbol{v}\times\boldsymbol{v} + \overline{m}g\hat{\boldsymbol{r}}_{\boldsymbol{p}}\boldsymbol{R^T}\boldsymbol{k}\\ &\quad + \boldsymbol{T_{ext}} - \hat{\boldsymbol{r}}_{\boldsymbol{p}}\overline{\boldsymbol{u}}\\ \overline{\boldsymbol{F}} &= (\boldsymbol{M}\boldsymbol{v} + \boldsymbol{P_p})\times\boldsymbol{\Omega} + m_0g\boldsymbol{R^T}\boldsymbol{k} + \boldsymbol{F_{ext}} - \overline{\boldsymbol{u}}.\end{aligned}$$

Here,

$$\begin{aligned}\boldsymbol{F_{ext}} &= \boldsymbol{R^T}\sum \boldsymbol{f_{ext_i}}\\ \boldsymbol{T_{ext}} &= \boldsymbol{R^T}\sum(\boldsymbol{x_i}-\boldsymbol{b})\times\boldsymbol{f_{ext_i}} + \boldsymbol{R^T}\sum \boldsymbol{\tau_{ext_j}}\end{aligned}$$

refer to external forces and moments, in this case lift and drag, with respect to the body frame.

B. Equations of Motion in the Vertical Plane

We now specialize the model to the vertical plane, the $\boldsymbol{i}$–$\boldsymbol{k}$ plane in inertial coordinates and the $\boldsymbol{e_1}$–$\boldsymbol{e_3}$ plane in body coordinates. Accordingly,

$$\boldsymbol{R} = \begin{pmatrix} \cos\theta & 0 & \sin\theta \\ 0 & 1 & 0 \\ -\sin\theta & 0 & \cos\theta \end{pmatrix} \qquad \boldsymbol{b} = \begin{pmatrix} x \\ 0 \\ z \end{pmatrix}$$

$$\boldsymbol{v} = \begin{pmatrix} v_1 \\ 0 \\ v_3 \end{pmatrix} \qquad \boldsymbol{\Omega} = \begin{pmatrix} 0 \\ \Omega_2 \\ 0 \end{pmatrix}$$

$$\boldsymbol{r_p} = \begin{pmatrix} r_{p1} \\ 0 \\ r_{p3} \end{pmatrix} \qquad \boldsymbol{P_p} = \begin{pmatrix} P_{p1} \\ 0 \\ P_{p3} \end{pmatrix} \qquad \overline{\boldsymbol{u}} = \begin{pmatrix} u_1 \\ 0 \\ u_3 \end{pmatrix}$$

where θ is pitch angle.

The equations of motion (18) for the gliding vehicle restricted to the vertical plane become

$$\dot{x} = v_1\cos\theta + v_3\sin\theta \tag{19}$$

$$\dot{z} = -v_1\sin\theta + v_3\cos\theta \tag{20}$$

$$\dot{\theta} = \Omega_2 \tag{21}$$

$$\dot{\Omega}_2 = \frac{1}{J_2}((m_3 - m_1)v_1v_3 - \overline{m}g(r_{P1}\cos\theta + r_{P3}\sin\theta) + M_{DL} - r_{P3}u_1 + r_{P1}u_3) \tag{22}$$

$$\dot{v}_1 = \frac{1}{m_1}(-m_3v_3\Omega_2 - P_{P3}\Omega_2 - m_0g\sin\theta + L\sin\alpha - D\cos\alpha - u_1) \tag{23}$$

$$\dot{v}_3 = \frac{1}{m_3}(m_1v_1\Omega_2 + P_{P1}\Omega_2 + m_0g\cos\theta - L\cos\alpha - D\sin\alpha - u_3) \tag{24}$$

$$\dot{r}_{P1} = \frac{1}{\overline{m}}P_{P1} - v_1 - r_{P3}\Omega_2 \tag{25}$$

$$\dot{r}_{P3} = \frac{1}{\overline{m}}P_{P3} - v_3 + r_{P1}\Omega_2 \tag{26}$$

$$\dot{P}_{P1} = u_1 \tag{27}$$

$$\dot{P}_{P3} = u_3 \tag{28}$$

$$\dot{m}_b = u_4. \tag{29}$$

Here, α is the angle of attack, D is drag, L is lift and M_{DL} is the viscous moment as shown in Fig. 5. These forces and moment are modeled as

$$D = (K_{D_0} + K_D\alpha^2)(v_1^2 + v_3^2)$$
$$L = (K_{L_0} + K_L\alpha)(v_1^2 + v_3^2)$$
$$M_{DL} = (K_{M_0} + K_M\alpha)(v_1^2 + v_3^2)$$

where the Ks are constant coefficients. This model is a standard one, derived using airfoil theory and potential flow calculations and then verified using experimental observations, see for example [12], [13]. The method for determination of the coefficients is described in Section III-C.

As shown in Fig. 5, we denote the glide path angle by ξ where

$$\xi = \theta - \alpha.$$

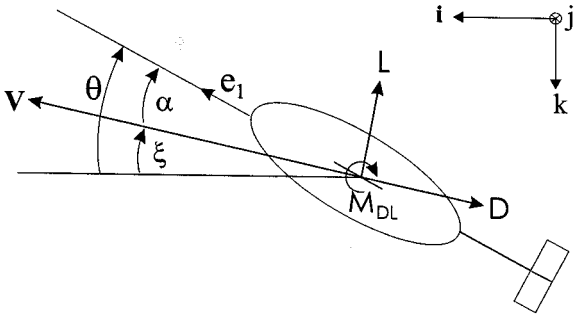

Fig. 5. Lift and drag on glider.

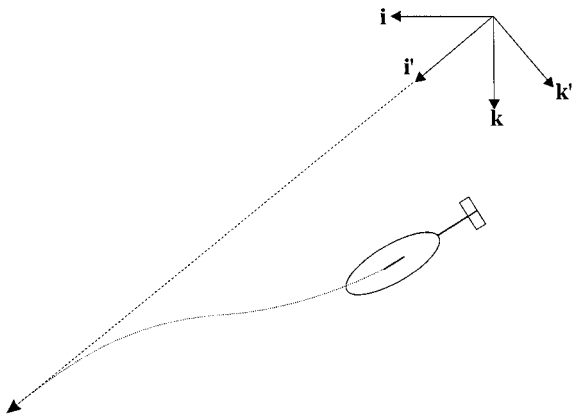

Fig. 6. Planar gliding controlled to a line.

We also denote the glider speed by V where

$$V = \sqrt{(v_1^2 + v_3^2)}.$$

We will typically specify a glide path by desired glide path angle ξ_d and desired speed V_d. We define inertial coordinates (x', z') such that x' coincides with the desired path:

$$\begin{pmatrix} x' \\ z' \end{pmatrix} = \begin{pmatrix} \cos\xi_d & -\sin\xi_d \\ \sin\xi_d & \cos\xi_d \end{pmatrix}\begin{pmatrix} x \\ z \end{pmatrix}. \tag{30}$$

Then, z' measures the vehicle's perpendicular distance to the desired path. We define two gliding objectives:

GO1 The objective is to control only the direction and speed of the vehicle's glide path. In this case we need not consider x and z at all.

GO2 The objective is to control gliding along a prescribed line (see Fig. 6). In this case we will include z' (but exclude x') in our analysis and we aim to make $z' = 0$.

The dynamics of the z' state are

$$\dot{z}' = \sin\xi_d(v_1\cos\theta + v_3\sin\theta) + \cos\xi_d(-v_1\sin\theta + v_3\cos\theta). \tag{31}$$

In the above model, the movable point mass can be controlled in all directions (2 degrees of freedom in the planar case). However, it may sometimes be the case that control over the CG location is restricted, for example, a battery may be shifted in a limited way. For the planar case, this might translate into a movable point mass with only one degree of freedom. To model this

we consider the case in which r_{P3} is fixed ($\dot{r}_{P3} = 0$), i.e., we can only move the point mass $\overline{m}$ in the $\boldsymbol{e_1}$ direction. Then

$$P_{P3} = \overline{m}(v_3 - r_{P1}\Omega_2). \tag{32}$$

The new equations of motion are (19)–(29) excluding (26) and (28). Further, P_{P3} is replaced by (32) and u_3 is replaced by $\dot{P}_{P3}$ which is computed by differentiating (32) with respect to time. In particular, (22) and (24) are replaced with

$$\begin{pmatrix} \dot{\Omega}_2 \\ \dot{v}_3 \end{pmatrix} = \boldsymbol{Z}^{-1} \begin{pmatrix} \frac{1}{J_2}\left(f_1 + r_{P1}\overline{m}\Omega_2\dot{r}_{P1}\right) \\ \frac{1}{m_3}\left(f_2 - \overline{m}\Omega_2\dot{r}_{P1}\right) \end{pmatrix}$$

where

$$\begin{aligned} f_1 &= (m_3 - m_1)v_1v_3 - \overline{m}g(r_{P1}\cos\theta + r_{P3}\sin\theta) \\ &\quad + M_{DL} - r_{P3}u_1 \\ f_2 &= m_1v_1\Omega_2 + P_{P1}\Omega_2 + m_0g\cos\theta - L\cos\alpha - D\sin\alpha \end{aligned}$$

$$\boldsymbol{Z} = \begin{pmatrix} 1 + \frac{\overline{m}r_{P1}^2}{J_2} & -\frac{\overline{m}r_{P1}}{J_2} \\ -\frac{\overline{m}r_{P1}}{m_3} & 1 + \frac{\overline{m}}{m_3} \end{pmatrix}.$$

III. Controllability of Steady Glide Paths

In this section, we compute steady glide paths. We then study controllability and observability of these glide paths.

A. Gliding Equilibria

We prescribe a desired glide path by specifying the desired glide path angle ξ_d and the desired speed V_d. We denote with subscript "d" the value of all dynamic variables at the glide equilibria. To get the conditions for such planar gliding equilibria, we set the left hand side of (31) and (21)–(29) to zero. This gives

$$\begin{aligned} 0 &= \sin\xi_d(v_{1_d}\cos\theta_d + v_{3_d}\sin\theta_d) \\ &\quad + \cos\xi_d(-v_{1_d}\sin\theta_d + v_{3_d}\cos\theta_d) && (33) \\ 0 &= \frac{1}{J_2}\left((m_{f3} - m_{f1})v_{1_d}v_{3_d}\right. \\ &\quad \left. - \overline{m}g(r_{P1_d}\cos\theta_d + r_{P3_d}\sin\theta_d) + M_{DL_d}\right) && (34) \\ 0 &= \frac{1}{m_{1_d}}\left(-m_{0_d}g\sin\theta_d + L_d\sin\alpha_d - D_d\cos\alpha_d\right) && (35) \\ 0 &= \frac{1}{m_{3_d}}\left(m_{0_d}g\cos\theta_d - L_d\cos\alpha_d - D_d\sin\alpha_d\right) && (36) \\ 0 &= \frac{1}{\overline{m}}P_{P1_d} - v_{1_d} && (37) \\ 0 &= \frac{1}{\overline{m}}P_{P3_d} - v_{3_d} && (38) \end{aligned}$$

and $z_d' = \Omega_{2_d} = u_{1_d} = u_{3_d} = u_{4_d} = 0$. Note that

$$\begin{aligned} m_{1_d} &= m_{b_d} + m_h + m_{f1}, \\ m_{3_d} &= m_{b_d} + m_h + m_{f3}, \\ m_{0_d} &= m_{b_d} + m_h + \overline{m} - m, \end{aligned}$$

which are all dependent on the equilibrium value of the variable mass m_{b_d}.

Given ξ_d, (35) and (36) may be solved for α_d. We can then compute

$$\begin{aligned} &\theta_d = \xi_d + \alpha_d, \qquad v_{1_d} = V_d\cos\alpha_d, \qquad v_{3_d} = V_d\sin\alpha_d, \\ &P_{P1_d} = \overline{m}v_{1_d}, \qquad P_{P3_d} = \overline{m}v_{3_d}. \end{aligned}$$

m_{b_d} can then be solved again using (35) and (36). Finally, (34) gives a one-parameter family of solutions for $(r_{P1_d}, r_{P3_d})^T$.

First, we compute α_d from (35) and (36). Note that these equations reduce to

$$\begin{aligned} &\begin{pmatrix} 0 \\ m_{0_d}g \end{pmatrix} \\ &\quad = \begin{pmatrix} \cos\theta_d & \sin\theta_d \\ -\sin\theta_d & \cos\theta_d \end{pmatrix}\begin{pmatrix} \cos\alpha_d & -\sin\alpha_d \\ \sin\alpha_d & \cos\alpha_d \end{pmatrix}\begin{pmatrix} D_d \\ L_d \end{pmatrix} \\ &\quad = \begin{pmatrix} \cos\xi_d & \sin\xi_d \\ -\sin\xi_d & \cos\xi_d \end{pmatrix}\begin{pmatrix} K_{D_0} + K_D\alpha_d^2 \\ K_{L_0} + K_L\alpha_d \end{pmatrix}V_d^2. \end{aligned} \tag{39}$$

The first equation of (39) is a quadratic equation in α_d. Provided $V_d \neq 0$ and $\xi_d \neq \pm(\pi/2)$, we have

$$\alpha_d^2 + \frac{K_L}{K_D}\tan\xi_d\alpha_d + \frac{1}{K_D}\left(K_{D_0} + K_{L_0}\tan\xi_d\right) = 0. \tag{40}$$

Equation (40) may be solved for a realizable α_d provided

$$\left(\frac{K_L}{K_D}\tan\xi_d\right)^2 - \frac{4}{K_D}\left(K_{D_0} + K_{L_0}\tan\xi_d\right) \geq 0. \tag{41}$$

Evaluating (41) for permissible values of ξ_d in the range $(-\pi/2, \pi/2)$, we see that we must choose

$$\xi_d \in \left(\tan^{-1}\left(2\frac{K_D}{K_L}\left(\frac{K_{L_0}}{K_L} + \sqrt{\left(\frac{K_{L_0}}{K_L}\right)^2 + \frac{K_{D_0}}{K_D}}\right)\right), \frac{\pi}{2}\right)$$

or

$$\xi_d \in \left(-\frac{\pi}{2}, \tan^{-1}\left(2\frac{K_D}{K_L}\left(\frac{K_{L_0}}{K_L} - \sqrt{\left(\frac{K_{L_0}}{K_L}\right)^2 + \frac{K_{D_0}}{K_D}}\right)\right)\right).$$

Since the drag model is valid only at small angles of attack, we take α_d as the solution of (41) with smaller magnitude,

$$\begin{aligned} \alpha_d &= \frac{1}{2}\frac{K_L}{K_D}\tan\xi_d \\ &\quad \times \left(-1 + \sqrt{1 - 4\frac{K_D}{K_L^2}\cot\xi_d(K_{D_0}\cot\xi_d + K_{L_0})}\right). \end{aligned} \tag{42}$$

If $\xi_d = \pm\pi/2$, then we simply have

$$\alpha_d = -\frac{K_{L_0}}{K_L}. \tag{43}$$

For a vehicle which is symmetric about the body $\boldsymbol{e_1}$–$\boldsymbol{e_2}$ plane, $K_{L_0} = 0$. In this case, for equilibria corresponding to vertical flight ($\xi_d = \pm\pi/2$), the desired angle of attack is zero.

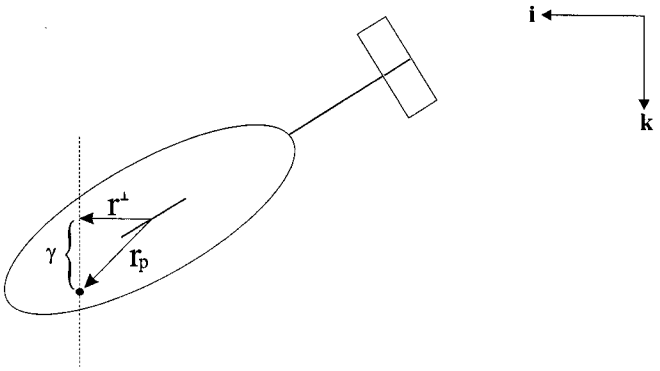

Fig. 7. Family of possible movable mass locations for a steady glide.

We may determine m_{b_d} from the latter equation in (39) as

$$m_{b_d} = (m - m_h - \overline{m}) + \frac{1}{g}(-\sin\xi_d(K_{D_0} + K_D\alpha_d^2) + \cos\xi_d(K_{L_0} + K_L\alpha_d))V_d^2. \tag{44}$$

Finally, we may solve for a one-parameter family of sliding mass locations $(r_{P1_d}, r_{P3_d})^T$ which satisfy (34). The family of solutions is

$$\boldsymbol{r_{Pd}} = \boldsymbol{r}^{\perp} + \gamma \begin{pmatrix} -\sin\theta_d \\ \cos\theta_d \end{pmatrix} \tag{45}$$

where

$$\boldsymbol{r}^{\perp} = \frac{1}{\overline{m}g}((m_{f3} - m_{f1})v_{1_d}v_{3_d} + (K_{M_0} + K_M\alpha_d)V_d^2) \times \begin{pmatrix} \cos\theta_d \\ \sin\theta_d \end{pmatrix}$$

and where γ is a real number. The vector $\boldsymbol{r}^{\perp}$ is a particular solution of (34). Since $(-\sin\theta, \cos\theta)^T = (\boldsymbol{R^T k})$ is the direction of gravity in body coordinates, $\boldsymbol{r}^{\perp}$ is orthogonal to the direction of gravity and γ measures the vehicle's "bottom-heaviness" as shown in Fig. 7.

For an experimental vehicle, r_{P3} may be a more physically relevant choice of parameter than γ. In this case,

$$r_{P1_d} = -r_{P3_d}\tan\theta_d + \frac{1}{\overline{m}g\cos\theta_d} \times ((m_{f3} - m_{f1})v_{1_d}v_{3_d} + (K_{M_0} + K_M\alpha_d)V_d^2) \tag{46}$$

for a given value of the parameter r_{P3_d}, provided $\theta_d \neq \pm\pi/2$. If $\theta_d = \pm\pi/2$, there is an equilibrium of the desired form if and only if the parameter r_{P3_d} satisfies

$$r_{P3_d} = \frac{1}{\overline{m}g\sin\theta_d}((m_{f3} - m_{f1})v_{1_d}v_{3_d} + (K_{M_0} + K_M\alpha_d)V_d^2). \tag{47}$$

If (47) is satisfied, r_{P1_d} is a free parameter. In fact, we should not choose r_{P3_d} to satisfy condition (47) in general because this will require that r_{P3_d} be small. Since r_{P3_d} contributes to the vehicle's "bottom-heaviness" at shallower glide path angles, satisfying condition (47) will affect stability of these other equilibria. [For a vehicle symmetric about the body $\boldsymbol{e_1}$–$\boldsymbol{e_2}$ plane, $\theta_d = \pm\pi/2$ implies that $K_{M_0} = 0$ and $\alpha_d = 0$. In this case, condition (47) requires that $r_{P3_d} = 0$.]

B. Linearization

We determine the linearization for the planar glider about a steady glide path.

Let $\boldsymbol{x} = (z', \theta, \Omega_2, v_1, v_3, r_{p_1}, r_{p_3}, P_{P_1}, P_{P_3}, m_b)^T$ and let $\boldsymbol{u} = (u_1, u_3, u_4)^T$. Define

$$\boldsymbol{\delta x} = \boldsymbol{x} - \boldsymbol{x_d}$$
$$\boldsymbol{\delta u} = \boldsymbol{u} - \boldsymbol{u_d}.$$

Then the linearized system is

$$\boldsymbol{\delta\dot{x}} = \boldsymbol{A\delta x} + \boldsymbol{B\delta u} \tag{48}$$

where $\boldsymbol{A}$ and $\boldsymbol{B}$ are defined as shown in (49) and (50), shown at the bottom of the next page. Here,

$$\begin{aligned}
\alpha_{v_1} &= -\frac{v_3}{V^2} \\
\alpha_{v_3} &= \frac{v_1}{V^2} \\
D_{v_1} &= (K_{D_0} + K_D\alpha^2)(2v_1) - 2K_D\alpha v_3 \\
D_{v_3} &= (K_{D_0} + K_D\alpha^2)(2v_3) + 2K_D\alpha v_1 \\
L_{v_1} &= (K_{L_0} + K_L\alpha)(2v_1) - K_L v_3 \\
L_{v_3} &= (K_{L_0} + K_L\alpha)(2v_3) + K_L v_1 \\
M_{v_1} &= (K_{M_0} + K_M\alpha)(2v_1) - K_M v_3 \\
M_{v_3} &= (K_{M_0} + K_M\alpha)(2v_3) + K_M v_1
\end{aligned}$$

where we have abbreviated $\partial\alpha/\partial v_1$ as α_{v_1}, etc., and

$$\begin{aligned}
a_{32} &= \frac{\overline{m}g}{J_2}(r_{P1_d}\sin\theta_d - r_{P3_d}\cos\theta_d) = \frac{\overline{m}g}{J_2}(-\gamma) \\
a_{34} &= \frac{1}{J_2}((m_{f3} - m_{f1})v_{3_d} + M_{v_1}|_{eq}) \\
a_{35} &= \frac{1}{J_2}((m_{f3} - m_{f1})v_{1_d} + M_{v_3}|_{eq}) \\
a_{42} &= -\frac{m_{0_d}}{m_{1_d}}g\cos\theta_d \\
a_{43} &= -\frac{m_{3_d} + \overline{m}}{m_{1_d}}v_{3_d} \\
a_{44} &= \frac{1}{m_{1_d}}(L_{v_1}\sin\alpha + L\cos\alpha\alpha_{v_1} - D_{v_1}\cos\alpha + D\sin\alpha\alpha_{v_1})_{eq} \\
a_{45} &= \frac{1}{m_{1_d}}(L_{v_3}\sin\alpha + L\cos\alpha\alpha_{v_3} - D_{v_3}\cos\alpha + D\sin\alpha\alpha_{v_3})_{eq} \\
a_{410} &= -\frac{g\sin\theta_d}{m_{1_d}} \\
a_{52} &= -\frac{m_{0_d}}{m_{3_d}}g\sin\theta_d \\
a_{53} &= \frac{m_{1_d} + \overline{m}}{m_{3_d}}v_{1_d} \\
a_{54} &= \frac{1}{m_{3_d}}(-L_{v_1}\cos\alpha + L\sin\alpha\alpha_{v_1} - D_{v_1}\sin\alpha - D\cos\alpha\alpha_{v_1})_{eq} \\
a_{55} &= \frac{1}{m_{3_d}}(-L_{v_3}\cos\alpha + L\sin\alpha\alpha_{v_3} - D_{v_3}\sin\alpha - D\cos\alpha\alpha_{v_3})_{eq} \\
a_{510} &= \frac{g\cos\theta_d}{m_{3_d}}.
\end{aligned}$$

The notation $(\cdot)|_{eq}$ indicates that the quantity is to be evaluated at the desired equilibrium.

This linearization can be used to check features of a given vehicle design, e.g., to check stability or controllability of a desired glide path given a choice of vehicle design parameters. One can also use this linearization to help automate the design procedure. For example, consider a vehicle that has been fully designed but for a choice of the position of the movable mass for a given glide path. Application of the Routh criterion to the characteristic polynomial of the matrix $\boldsymbol{A}$ gives conditions for stability of the glide path. These conditions can be written in terms of the free variable r_{P3}. r_{P3} would then be chosen for behavior with desired stability and r_{P1} would then be computed according to (46).

C. Controllability and Observability

In this section we describe controllability and observability of steady glide paths for a model of our experimental vehicle ROGUE. ROGUE has an ellipsoidal body with axes of length 18, 12, and 6 in. The wings are symmetric airfoils from [21] for low Reynolds number. We note that the body and wings have not been designed for optimal gliding performance but rather in consideration of available facilities and other manufacturing constraints. Each wing has span of 28 inches with aspect ratio 9.3. The glider body, wings and tail are all machined from UHMW (ultra-high molecular weight) plastic. Mass and inertia properties were measured directly. Added mass and inertia properties can be found, for example, in [20]. Lift and drag for the body were found experimentally as described in [8]. Lift and drag for the wings were taken from the data in [19]. Lift for the body plus wings was then computed using Schrenk's method [21], and drag was computed as the sum of the drag on the wing and the body. The lift moment was approximated by taking into account the tail. The vehicle model parameters are given as follows:

$$\begin{aligned} m &= 11.22 \text{ kg} \\ m_h &= 8.22 \text{ kg} \\ \overline{m} &= 2.0 \text{ kg} \\ m_{f1} &= 2 \text{ kg} \\ m_{f3} &= 14 \text{ kg} \\ J_2 &= 0.1 \text{ Nm}^2 \\ K_{D_0} &= 18 \text{ N(s/m)}^2 \\ K_D &= 109 \text{ N(s/m)}^2 \\ K_L &= 306 \text{ N(s/m)}^2 \\ K_M &= -36.5 \text{ Nm(s/m)}^2. \end{aligned}$$

$$\boldsymbol{A} = \begin{bmatrix} 0 & -V_d & 0 & -\sin\alpha_d & \cos\alpha_d & 0 & 0 & 0 & 0 & 0 \\ 0 & 0 & 1 & 0 & 0 & 0 & 0 & 0 & 0 & 0 \\ 0 & a_{32} & 0 & a_{34} & a_{35} & -\dfrac{\overline{m}g\cos\theta_d}{J_2} & -\dfrac{\overline{m}g\sin\theta_d}{J_2} & 0 & 0 & 0 \\ 0 & a_{42} & a_{43} & a_{44} & a_{45} & 0 & 0 & 0 & 0 & a_{410} \\ 0 & a_{52} & a_{53} & a_{54} & a_{55} & 0 & 0 & 0 & 0 & a_{510} \\ 0 & 0 & -r_{P3} & -1 & 0 & 0 & 0 & \dfrac{1}{\overline{m}} & 0 & 0 \\ 0 & 0 & r_{P1} & 0 & -1 & 0 & 0 & 0 & \dfrac{1}{\overline{m}} & 0 \\ 0 & 0 & 0 & 0 & 0 & 0 & 0 & 0 & 0 & 0 \\ 0 & 0 & 0 & 0 & 0 & 0 & 0 & 0 & 0 & 0 \\ 0 & 0 & 0 & 0 & 0 & 0 & 0 & 0 & 0 & 0 \end{bmatrix} \tag{49}$$

$$\boldsymbol{B} = \begin{bmatrix} 0 & 0 & 0 \\ 0 & 0 & 0 \\ -\dfrac{r_{P3_d}}{J_2} & \dfrac{r_{P1_d}}{J_2} & 0 \\ -\dfrac{1}{m_{b_d}+m_h+m_{f1}} & 0 & 0 \\ 0 & -\dfrac{1}{m_{b_d}+m_h+m_{f3}} & 0 \\ 0 & 0 & 0 \\ 0 & 0 & 0 \\ 1 & 0 & 0 \\ 0 & 1 & 0 \\ 0 & 0 & 1 \end{bmatrix} \tag{50}$$

The first three masses, m, m_b, and $\overline{m}$ were measured with a high degree of accuracy. The other terms have less precision because they are based on look up tables and approximation methods.

Four steady glide paths are calculated using the method of Section III-A. The glide paths are at glide angles $-30°$, $-45°$, $30°$ and $45°$. We compute the glide path at $-30°$ by choosing a desired glide speed $V_d = 0.30$ m/s and a desired vertical location of the movable mass given by $r_{P3_d} = 4$ cm. This results in an equilibrium variable mass given by $m_{b_d} = 1.36$ kg. The glide path at $-45°$ is computed for these same values of r_{P3_d} and m_{b_d}. The corresponding equilibrium speed for this glide is computed as $V_d = .37$ m/s. Similarly, we computed the two steady upward glide paths, for the same value of r_{P3_d} and the same buoyant force magnitude, i.e., the value of $|m_{0_d}|$ is held constant. Recall that m_0 is the mass of the vehicle m_v less the mass of the displaced fluid m. The full description of each of the four glide paths is given in Table II.

TABLE II
FOUR STEADY GLIDE PATHS FOR ROGUE

Variable	Down 30°	Down 45°	Up 30°	Up 45°
ξ_d (deg)	-30	-45	30	45
θ_d (deg)	-23.7	-41.5	23.7	41.5
α_d (deg)	6.3	3.5	-6.3	-3.5
V_d (m/s)	0.30	0.37	0.30	0.37
v_{1_d} (m/s)	0.29	0.36	0.29	0.36
v_{3_d} (m/s)	0.03	0.02	-0.03	-0.02
r_{P1_d} (cm)	0.41	2.20	-0.41	-2.20
r_{P3_d} (cm)	4.0	4.0	4.0	4.0
P_{P1_d} (kg-m/s)	0.60	0.73	0.60	0.73
P_{P3_d} (kg-m/s)	0.07	0.04	-0.07	-0.04
m_{b_d} (kg)	1.36	1.36	0.64	0.64
m_{0_d}(kg)	0.36	0.36	-0.36	-0.36

Local properties of these steady glide paths can be studied using the linearization of Section III-B. By plugging in the equilibrium values, we can examine the linearization for stability, controllability and observability. The four glide paths listed in Table II all have a relatively slow unstable mode. They are all, however, locally controllable. That is, $\boldsymbol{A}$ and $\boldsymbol{B}$ as given by (49) and (50), when evaluated at any of the four equilibria, satisfy the controllability rank condition. Note that the linearization includes the state z' meaning that controllability extends to the variable z'. Accordingly, we can successfully design a linear controller that will locally accomplish not only glide objective **GO1** but also **GO2**.

It is of interest to check the controllability rank condition in the case that the movable mass $\overline{m}$ can only move in one direction (i.e., r_{P3} is fixed). To do this we have linearized the equations of motion for the single degree-of-freedom moving mass described at the very end of Section II. Again the new $\boldsymbol{A}$ and $\boldsymbol{B}$ matrices for this case, when evaluated at any of the above four glide paths, satisfy the controllability rank condition. Thus, it seems that at least for linear type control action, not much is lost in restricting the degrees of freedom of the movable mass from two to one.

On the other hand, for large motions, such as switching from an upward to a downward glide path, care needs to be taken if restricting the degrees of freedom of the movable mass. For instance, while motion of the movable mass restricted to the r_{P1} direction would be sufficient for sawtooth maneuvers, motion restricted to the r_{P3} direction would not allow for both upward and downward glide motions. Because of the glider shape, mass motion restricted to the r_{P3} direction will also typically have more limited travel as compared to motion in the r_{P1} direction.

The movable mass $\overline{m}$ for ROGUE is approximately 1/6 of the vehicle displacement m. This is of the same relative order as the movable mass in the gliders SLOCUM, Spray and Seaglider. Variations in this mass or its location will not in principle affect local controllability of a feasible glide path. In practice, however, there are clear tradeoffs associated with moving a large mass a short distance versus moving a small mass a large distance. For example, a large mass may be energetically expensive to move and the necessary motion control resolution required may be difficult to achieve. On the other hand, since only short travel would be required, there would be a smaller demand on vehicle volume. Variation in mass and location will also affect the range of feasible glide paths and the nature of the switching between them. The variable mass m_{b_d} in ROGUE at the equilibrium described above is larger relative to vehicle displacement as compared to these other gliders. This mass controls glide speed; thus, for example, if significant vehicle load required designing for a smaller variable mass then maximum glide speed would be reduced.

Observability of the linearized model about the four glide paths listed in Table II was also investigated. If **GO1** is our objective, i.e., if we are interested in controlling only the direction and speed of the vehicle's glide path, then we need not measure z'. The nine-dimensional dynamic model (which excludes z') is completely observable with measurements limited to movable mass position r_{p1}, r_{p3} and variable mass m_b. In this case, pitch angle θ, pitch rate Ω_2, linear velocity components v_1 and v_3 and the momentum of the movable mass P_{p1}, P_{p3} need not be sensed. Observability means that with the measurements of r_{p1}, r_{p3} and m_b, a dynamic observer could be designed to give an estimate of the unmeasured states θ, Ω_2, v_1, v_3, P_{p1} and P_{p3}. Of course, θ is typically already measured and Ω_2 is not so hard to measure, so the real advantage is in the estimation of v_1, v_3, P_{p1} and P_{p3} which are more difficult to measure. The nine-dimensional dynamic model is also completely observable with measurements limited to θ, r_{p1} (or r_{p3}) and m_b. Again this means that using these three measurement signals, an observer could be designed to estimate the rest of the states.

If **GO2** is our objective, i.e., if we want to control the glider to a prescribed line in the plane, then we need a measurement of z'. Recall from (30) that z' depends on both depth z, which is easily measured, and horizontal position x, which is not so easily measured. The measurements r_{p1}, r_{p3} and m_b, together with a measurement of z (or alternatively θ, r_{p1}, m_b and z), do not render x observable. This means that without an initial condition measurement $x(0)$, the trajectory $x(t)$ can not be computed. However, with an initial measurement of x given say from a GPS fix taken when the glider is at the surface, the horizontal motion of the glider can be calculated, for example, by making use of the estimate of linear velocity $\boldsymbol{v}$ from the observer. We note that this approach has the potential to improve the accuracy of horizontal motion determination over current methods which are based on assumptions of constant angle of attack, etc. For example, on SLOCUM, the horizontal motion of the glider during the glide

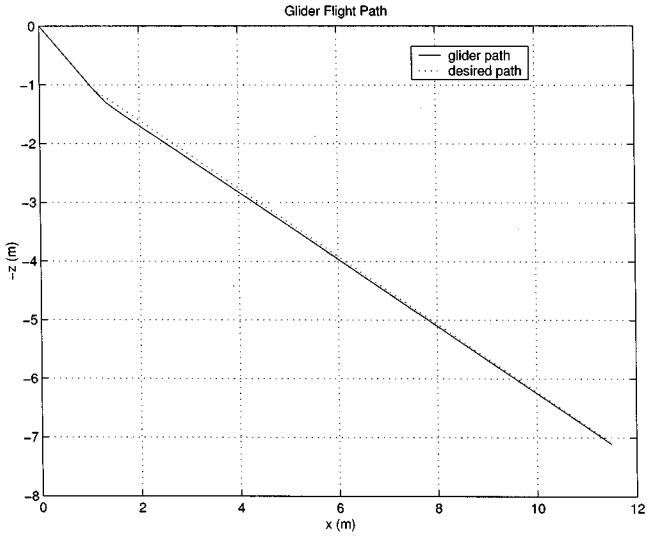

Fig. 8. Simulation of glide path from 45° downward to 30° downward.

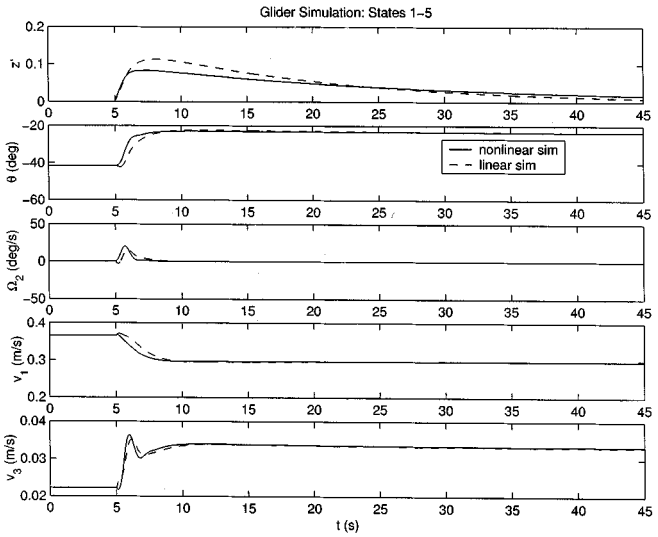

Fig. 9. Simulation of position and velocity variables.

is estimated from GPS fixes taken at the surface, measured pitch angle θ, an assumed angle of attack and vertical speed computed from depth measurements [6]. Similarly, on Spray, horizontal flight distance is calculated based on a constant pitch, heading and angle of attack to which the vehicle is being controlled [4].

IV. Controlled Planar Gliding

In this section we demonstrate, in simulation, controlled gliding in the vertical plane by designing and testing a linear controller for the glide path moving 30° downward as described in Table II. Since the controller is linear, we expect that it should take initial conditions nearby to the 30° downward glide path. We demonstrate this result by starting the glider at the 45° downward steady glide and using the linear controller to move it to the 30° downward glide solely by feedback.

The controller is designed for the linearization about the 30° downward glide using the LQR (linear quadratic regulator) method. This is a standard linear optimal control design method which produces a stabilizing control law that minimizes a cost function that is a weighted sum of the squares of the states and input variables. We assume that all of the states are available for feedback. If this were not the case, then, as described above, it is possible to design an estimator to determine the unmeasured states.

The cost function to be minimized is defined as

$$J = \int_0^\infty \boldsymbol{\delta x^T Q \delta x} + \boldsymbol{\delta u^T R \delta u}\, dt$$

where Q and R are state and control penalty matrices. Q and R were chosen to ensure well-behaved dynamics and to prevent large motions in the movable mass position and variable mass that would exceed physical limitations. Taking into account real or desirable maximum state values, the states associated with vehicle and movable mass velocity and variable mass and pitch angle were weighted most heavily. No significant tuning was performed. The weight selections are given by

$$\boldsymbol{Q} = \mathrm{diag}(0.05,\ 0.5,\ 1,\ 2,\ 2,\ 0.1,\ 0.1,\ 1,\ 1,\ 0.5),$$
$$\boldsymbol{R} = \mathrm{diag}(1,\ 1,\ 1).$$

The corresponding control law is $\boldsymbol{u} = -\boldsymbol{K}\boldsymbol{\delta x}$ where K is computed using MATLAB as the solution to the Riccati equation given $\boldsymbol{A}$, $\boldsymbol{B}$, $\boldsymbol{Q}$, $\boldsymbol{R}$.

In Figs. 8–10, we show a MATLAB simulation of the glider moving first along the 45° downward glide and then switching to the 30° downward glide path. This was accomplished by turning on the linear controller at $t = 5$ seconds. In Fig. 8 we show the glide path, in Fig. 9 we show plots of position, pitch, linear and angular velocity as a function of time and in Fig. 10 we show the position of the movable mass, the net buoyant force as well as the control inputs as a function of time. In these latter two figures we show the results of the controller as applied to the linear dynamic model and the results as applied to the nonlinear dynamic model.

The figures show that the 45° downward glide path is in the region of attraction of the linear controller designed for the 30° downward glide path. Furthermore, the transient is very well behaved.

However, we do not expect that the upward equilibria would be in the region of attraction of a linear controller designed for a downward glide (and vice-versa). This means we would not want to use a pure linear feedback solution for switching in a sawtooth glide path. Instead, we could consider complementing the feedback law with a feedforward term which drives the movable mass and the variable mass in a predetermined way from initial to final condition. Alternatively, we can consider a nonlinear control design approach that would include feedback and may or may not include a feedforward term. A feedforward term would make it possible to introduce an optimal path between two different glides.

Laboratory experiments of controlled gliding with ROGUE will be described in a future publication.

V. Final Remarks

We plan to realize the results described in this paper as well as future control design developments on experimental gliders both of our own construction, e.g., ROGUE, and with our colleagues who build sea-worthy gliders, e.g., SLOCUM.

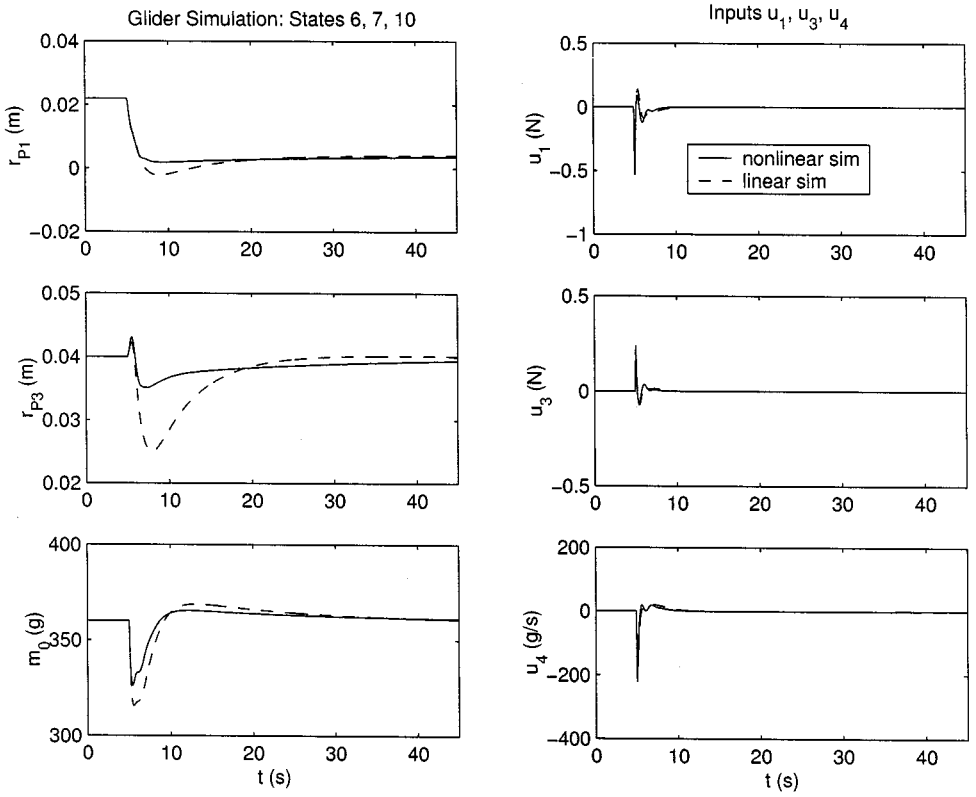

Fig. 10. Simulation of movable mass, variable mass, and control inputs.

In future work we intend to further develop the gliding control methodology by investigating nonlinear feedback control laws, feedforward control and path planning. We are already working with colleagues on optimal control theory that is applicable to underwater gliders [7] and that may be useful for path planning purposes.

Other future directions include extending our work to gliding motion in the horizontal plane, e.g., waypoint following, and to glider network maneuvers. Work is already underway to develop decentralized control laws to produce underwater vehicles that school [9], [10], and these we hope to integrate with control of glider dynamics. In support of this effort, we are building an experimental, underwater test-bed for multiple-vehicle control [22]. Schooling fish function like an integrated sensing system and by emulating their traffic rules, we can hope to produce a network of gliders that can similarly serve as a fast and effective adaptive ocean sensing platform.

ACKNOWLEDGMENT

The authors would like to thank M. Chyba, K. Pettersen, and C. Woolsey for helpful discussions on this work, and the anonymous reviewers for their motivating comments and suggestions.

REFERENCES

[1] T. B. Curtin, J. G. Bellingham, J. Catipovic, and D. Webb, "Autonomous oceanographic sampling networks," *Oceanography*, vol. 6, no. 3, pp. 86–94, 1989.

[2] H. Stommel, "The Slocum mission," *Oceanography*, vol. 2, no. 1, pp. 22–25, 1989.

[3] D. C. Webb, P. J. Simonetti, and C. P. Jones, "SLOCUM, an underwater glider propelled by environmental energy," *IEEE J. Oceanic Eng.*, vol. 26, pp. XX–XX, Oct. 2001.

[4] J. Sherman, R. E. Davis, W. B. Owens, and J. Valdes, "The autonomous underwater glider 'Spray'," *IEEE J. Oceanic Eng.*, vol. 26, pp. 437–446, Oct. 2001.

[5] C. C. Eriksen, T. J. Osse, R. Light, R. D. Wen, T. W. Lehmann, P. L. Sabin, J. W. Ballard, and A. M. Chiodi, "Seaglider: A long range autonomous underwater vehicle for oceanographic research," *IEEE J. Oceanic Eng.*, vol. 26, pp. 424–436, Oct. 2001.

[6] D. Webb and C. Jones, "Personal communication," unpublished, 2001.

[7] M. Chyba, N. E. Leonard, and E. D. Sontag, "Optimality for underwater vehicles," in *Proc. IEEE Conf. on Decision and Control*, 2001, submitted for publication.

[8] J. Graver, J. Liu, C. Woolsey, and N. E. Leonard, "Design and analysis of an underwater vehicle for controlled gliding," in *Proc. 32nd Conf. on Information Sciences and Systems*, 1998, pp. 801–806.

[9] N. E. Leonard and E. Fiorelli, "Virtual leaders, artificial potentials and coordinated control of groups," in *Proc. IEEE Conf. Decision and Control*, 2001.

[10] T. R. Smith, H. Hanßmann, and N. E. Leonard, "Orientation control of multiple underwater vehicles with symmetry-breaking potentials," in *Proc. IEEE Conf. Decision and Control*, 2001.

[11] J. P. Campbell and M. O. McKinney, "Summary of methods for calculating dynamic lateral stability and response and for estimating lateral stability derivatives,", Tech. Rep., NACA R 1098, 1952.

[12] B. Etkin, *Dynamics of Flight*. New York: Wiley, 1959.

[13] B. W. McCormick, *Aerodynamics, Aeronautics and Flight Mechanics*. New York: Wiley, 1979.

[14] C. D. Perkins and R. E. Hage, *Airplane Performance, Stability and Control*. New York: Wiley, 1949.

[15] J. Roskam, *Methods for Estimating Stability and Control Derivatives of Conventional Subsonic Airplanes*. Lawrence, KS: J. Roskam, 1971.

[16] ——, *Flight Dynamics of Rigid and Elastic Airplanes*. Lawrence, KS: J. Roskam, 1973.

[17] H. Goldstein, *Classical Mechanics*, 2nd ed. Reading, MA: Addison-Wesley, 1980.

[18] H. Lamb, *Hydrodynamics*, 6th ed. New York: Dover, 1932.

[19] M. S. Selig, J. F. Donovan, and D. B. Fraser, *Airfoils at Low Speeds*. Virginia Beach, VA: H. A. Stokely, 1989.

[20] I. A. Kibel, N. E. Kochen, and N. V. Roze, *Theoretical Hydromechanics*. New York: Wiley, 1964.
[21] O. Schrenk, "A simple approximation method for obtaining spanwise lift distribution,", Tech. Rep., NACA, 1940.
[22] R. Bachmayer and N. E. Leonard, "Experimental test-bed for multi-vehicle control, navigation and communication," in *Proc. 12th Int. Symp. Unmanned Untethered Submersible Tech.*, Durham, NH, 2001.

Naomi E. Leonard received the B.S.E. degree in mechanical engineering from Princeton University, Princeton, NJ, in 1985 and the M.S. and Ph.D. degrees in electrical engineering, from the University of Maryland, College Park, in 1991 and 1994, respectively.

She is an Associate Professor of Mechanical and Aerospace Engineering at Princeton University. She is also an Associated Faculty member of the Program in Applied and Computational Mathematics at Princeton. From 1985 to 1989, she worked as an engineer in the electric power industry for MPR Associates, Inc., Alexandria, VA. Her research interests include dynamics and control of nonlinear systems with application to mechanical systems such as autonomous underwater vehicles. In 2000, she was the Applied Ocean Science and Engineering Visiting Scholar at the Woods Hole Oceanographic Institution, and in 2001, she was the Lise Meitner Guest Professor at Lund University in Sweden.

Prof. Leonard is a recipient of a National Science Foundation CAREER award (1995), an Office of Naval Research Young Investigator Program Award (1998), and an *Automatica* Prize Paper Award (1999).

Joshua G. Graver received the B.S.E. and M.A. degrees in mechanical and aerospace engineering from Princeton University, Princeton, NJ, in 1998, and 2000, respectively. His undergraduate thesis involved the design and construction of a laboratory scale underwater glider. He is currently working toward the Ph.D. degree in the Dynamical Control Systems Laboratory, at the same university.

His research includes underwater vehicle and glider design, dynamics and control. He has built several laboratory scale underwater vehicles. His other interests include aircraft dynamics and the use of robotics in hostile environments.